NREL
NATIONAL RENEWABLE ENERGY LABORATORY

Quantitative Analysis of Spectral Impacts on Silicon Photodiode Radiometers

Preprint

D. R. Myers

To be presented at SOLAR 2011
Raleigh, North Carolina
May 17–21, 2011

Conference Paper
NREL/CP-5500-50936
April 2011

Contract No. DE-AC36-08GO28308

NOTICE

Available electronically at http://www.osti.gov/bridge

Available for a processing fee to U.S. Department of Energy
and its contractors, in paper, from:

U.S. Department of Energy
Office of Scientific and Technical Information

P.O. Box 62
Oak Ridge, TN 37831-0062
phone: 865.576.8401
fax: 865.576.5728
email: mailto:reports@adonis.osti.gov

Available for sale to the public, in paper, from:

U.S. Department of Commerce
National Technical Information Service
5285 Port Royal Road
Springfield, VA 22161
phone: 800.553.6847
fax: 703.605.6900
email: orders@ntis.fedworld.gov
online ordering: http://www.ntis.gov/help/ordermethods.aspx

Cover Photos: (left to right) PIX 16416, PIX 17423, PIX 16560, PIX 17613, PIX 17436, PIX 17721

Printed on paper containing at least 50% wastepaper, including 10% post consumer waste.

QUANTITATIVE ANALYSIS OF SPECTRAL IMPACTS ON SILICON PHOTODIODE RADIOMETERS

Daryl R. Myers
National Renewable Energy Laboratory
1617 Cole Blvd. MS 3411
Golden, CO 80401
e-mail: daryl.myers@nrel.gov

ABSTRACT

Inexpensive broadband pyranometers with silicon photodiode detectors have a non-uniform spectral response over the spectral range of 300–1100 nm. The response region includes only about 70% to 75% of the total energy in the terrestrial solar spectral distribution from 300 nm to 4000 nm. The solar spectrum constantly changes with solar position and atmospheric conditions. Relative spectral distributions of diffuse hemispherical irradiance sky radiation and total global hemispherical irradiance are drastically different. This analysis convolves a typical photodiode response with SMARTS 2.9.5 spectral model spectra for different sites and atmospheric conditions. Differences in solar component spectra lead to differences on the order of 2% in global hemispherical and 5% or more in diffuse hemispherical irradiances from silicon radiometers. The result is that errors of more than 7% can occur in the computation of direct normal irradiance from global hemispherical irradiance and diffuse hemispherical irradiance using these radiometers.

1. INTRODUCTION

The growth of interest in "bankable" solar resource data for the justification of solar energy conversion system financing has raised a question regarding the quality of measured and modeled solar radiation resource data. Inexpensive silicon photodiode (PD) radiometers (pyranometers) for measuring total hemispherical solar radiation on a horizontal ("global horizontal") or tilted (plane of array) surface are popular because of their low cost. These radiometers have a long history of characterization with respect to their response characteristics and accuracy in general (1, 2, 3). Here, the spectral response issue is specifically studied, as it has a fundamental impact on the performance of rotating shadowband radiometers. Rotating shadowband radiometers use measurements of two solar radiation components, total hemispherical radiation and diffuse hemispherical radiation on a horizontal surface, to compute direct beam irradiance. Each of these components has a distinct spectral distribution, which contributes to the overall errors in each reported solar radiation component.

Mention of specific instrumentation does not imply endorsement or recommendations regarding such instrumentation.

2. APPROACH

Because of their wide spectral response regime (typically 300–2400 nm), pyranometers and pyrheliometers using thermal detectors have long been considered the most accurate instruments for measuring solar radiation (4, 5). Lower-cost silicon PD radiometers are popular for monitoring global hemispherical irradiance (GHI) and plane of array irradiance for solar conversion systems. PD radiometers also provide a relatively inexpensive means of estimating direct beam irradiance (direct normal irradiance, or DNI) using a rotating shadowband radiometer (6).

This analysis uses the spectral response for a typical PD radiometer (Li-Cor LI 200 SA pyranometer) in conjunction with modeled clear sky spectral distributions. The distributions are modeled using Gueymard's SMARTS spectral model, version 2.9.5 (7). Spectral distributions representative of different atmospheric conditions and locations are used to compute the "effective irradiance" or actual irradiance sensed by the silicon PD. Effective irradiance is the integral of the convolution of the PD spectral response and the solar spectral distribution. (See Fig. 1.)

By integrating the complete spectral distribution, the total irradiance available for a conversion system can be calculated. Typically, a "calibration" of a PD pyranometer compares the output, based on the effective irradiance, with the total irradiance measured with a thermal detector radiometer, such as an Eppley Laboratories Model PSP, Kipp and Zonen CM11, or other model pyranometer. These thermal detectors are calibrated to represent the total irradiance, or total integral of the prevailing spectral distribution. This analysis examines the relationship between the effective irradiance and total irradiance as a function of the changing spectral distributions during calibration and the routine measurement process.

3. SPECTRAL VARIABILITY AND EFFECTIVE IRRADIANCE

Fig. 1 shows the spectral response of the LI-Cor LI 200 SA pyranometer as obtained by digitizing Fig. 5 in (8). Also shown are sea-level GHI SMARTS spectra as a function of air mass (AM) as the atmospheric path length increases from AM 1.1 to am 5.0, with rural aerosol optical depth 0.1 and total precipitable water 2.5 atm-cm.

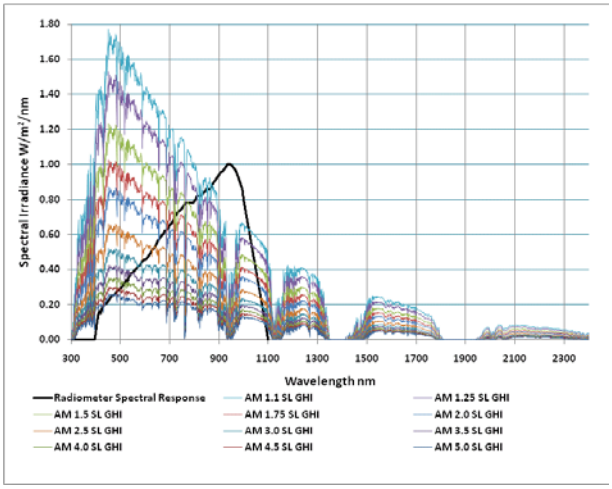

Fig. 1: Spectral variations at sea level as a function of air mass with total precipitable water 2.5 atm-cm and aerosol optical depth 0.10.

In contrast, Fig. 2 shows the portion of the diffuse horizontal irradiance (DHI) spectral distribution not sensed by the silicon PD at sea level (lower set of thin curves) compared with the DHI at the National Renewable Energy Laboratory in Golden, Colorado, at an altitude of 1800 m, with a station pressure of 820 mB, aerosol optical depth of 0.05, and precipitable water of 0.5 atm-cm.

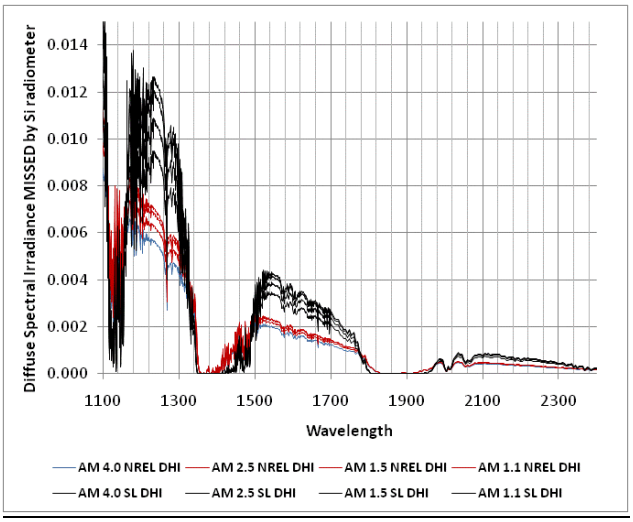

Fig. 2: DHI not sensed by silicon PD at sea level (upper four curves) compared with Golden, Colorado, at 1800 m.

The lack of sensitivity of the silicon PD radiometer to these spectral differences means the integrated energy beyond 1100 nm cannot be deduced from a shaded PD radiometer. Corrections derived from King (2), Vignola (3), and others (9) are applied to shaded PD signals corresponding to where the sensor responds, but the corrections do not address these spectral differences. The spectral differences in the GHI are not as pronounced, as shown in Fig. 3, but are still apparent.

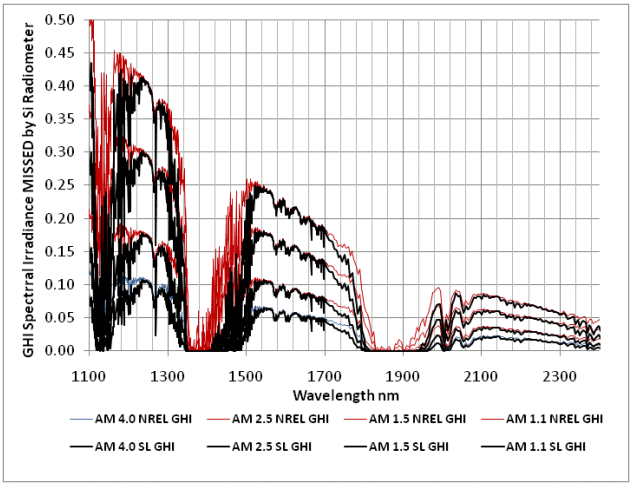

Fig. 3: GHI not sensed by silicon PD at sea level (thick curves) compared with Golden, Colorado (thin curves).

The reason for the spectral differences between the high-elevation and sea-level spectra is the different atmospheric transmittance because of more or less atmosphere, aerosols, and water vapor. The water vapor absorption bands at 1100 nm, 1400 nm, and 1900 nm are well outside the response region of the silicon PD radiometer. Variations in water vapor result in changes in the depth and width of these absorption bands that are not detectable by the silicon PD radiometer.

In contrast, Fig. 4 shows the effective GHI and effective DHI sensed by the silicon PD at AM 1.5 and AM 3.0 at sea level and the Golden, Colorado, site. By comparing the relative contribution of the integrated effective DHI and GHI with the integrated total GHI and DHI for these sites and a range of air mass and atmospheric conditions, it will be shown how the error in DNI derived from rotating shadowband radiometers measurement systems can vary.

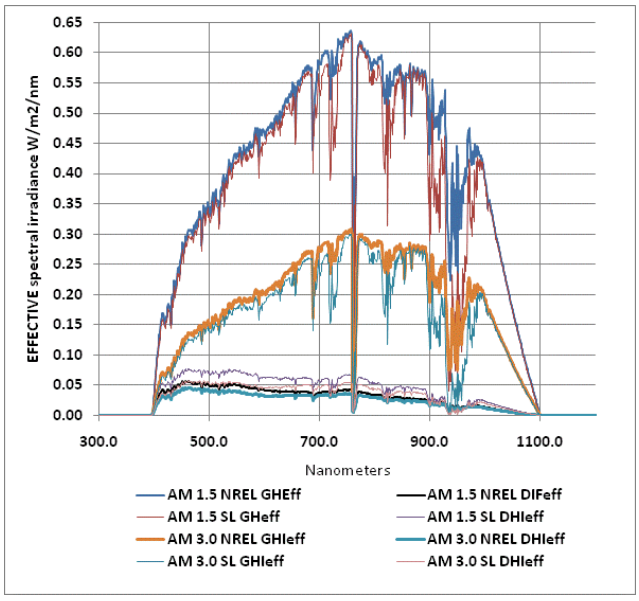

Fig. 4. Effective GHI and DHI for sea level (thin lines) and Golden, Colorado, (thick lines) for AM 1.5 and AM 3.0 and conditions in Table 1.

4. STUDY CONDITIONS AND ANALYSIS

Table 1 displays the conditions analyzed for the relative contribution of spectral error to GHI, DHI, and rotating shadowband radiometer computed DNI irradiances.

For each of the conditions, at each geometrical air mass specified in Table 1 (1.10, 1.25, 1.50, 1.75, 2.00, 2.50, 3.00, 3.50, 4.00, 4.50, and 5.0), the following are performed:

- Integrate total GHI spectrum 300 nm–4000 nm
- Integrate total DHI spectrum
- Integrate effective GHI spectrum 300 nm–1100 nm
- Integrate effective DHI spectrum.

TABLE 1. STUDY CONDITIONS

Site	Golden, Colorado	Sea Level
Elevation	1800 m	0 m
Aerosol optical depth	0.05	0.1
Precipitable water atm-cm	0.5	2.5
Aerosol profile	Rural	Rural
Geometrical air mass	1.25 to 5.0	1.25 to 5.0

Using these integrals, the ratios of effective irradiances to total integrated irradiances are computed and plotted as a function of air mass, as in Fig 5.

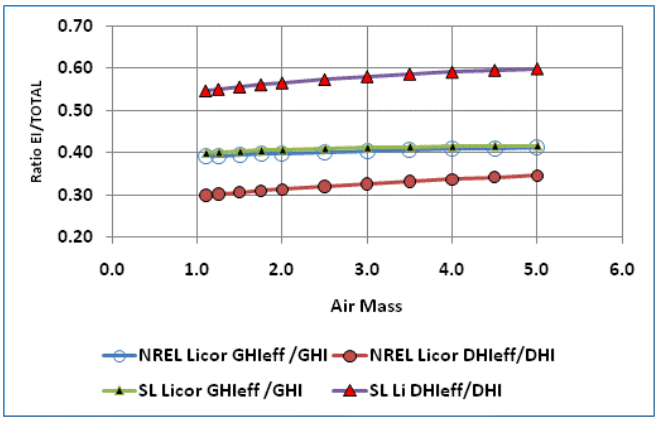

Fig. 5. Ratio of clear sky effective GHI/GHI and effective DHI/DHI for sea level and Golden, Colorado, as a function of air mass. Note that the GHI curves are practically identical and the DHI curves are significantly different for the two locations. (TOTAL refers to the respective GHI or DHI total integral.)

The important aspect of Fig. 5 is that the relative contributions of the effective diffuse irradiances to the total diffuse irradiance are significantly different at the two sites. The sea-level DHI ratio has a slightly greater nonlinear (more curvature) dependence on air mass than the Golden, Colorado, data. The relative error in "raw" DHI (shaded silicon pyranometer) for a sea level site is about 55%, while at the high-altitude Golden site, the relative error in "raw" shaded silicon detector data is only about 35%. *The difference between any average correction factors needed to accurately estimate total DHI at each site is almost 60%.*

To further emphasize differences in the relationship of the effective GHI and DHI irradiances to the total irradiances at

each site, Fig. 6 shows the ratio of the sea level to Golden, Colorado, effective to total ratios. For example:

[(DHIeff/DHI) at sea level] / [(DHIeff/DHI) at Golden].

Note the right (red) scale of Fig. 6 relates to the GHI ratios, and has a range of variation of only 1.4%. The ratio of GHI ratios at the two sites is nonlinear with air mass. However, the left scale (black) relates to the DHI ratios and has a range of variation of about 6%. The ratio of the DHI ratios appears to be linear with air mass. Empirical DHI corrections derived (e.g., by comparison with total diffuse measured with a thermal pyranometer) and applied at one site will generally not apply at the other. Also, corrections to GHI data applied to DHI data could be off by factors as large as 6 at higher air masses.

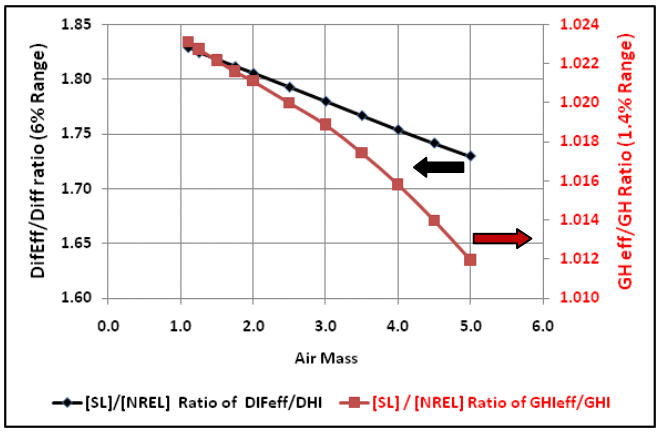

Fig 6. Plot of the ratios of the effective to total GHI and DHI ratios at Golden, Colorado, and sea level ratioed to each other, as a function of air mass.

Given that there can be a 60% difference in a DHI correction factor of about 40% between a seal-level site and a high-altitude site such as Golden, Colorado, the net effect can be errors on the order of 0.6 x 0.4 or 0.25, or 25% in the corrected DHI data.

For clear skies, where DHI is about 10% to 15% of the GHI, rotating shadowband radiometer instruments compute DNI from (GHI-DHIcorrected) / cos(z). If there is a 1.5% "error" in GHI (e.g., as in Fig. 6) and a 50% error in DHI correction when the DHI is ~15% of the total, then the DHI contribution to the error in computing DNI, as a percentage of the total GHI, becomes 0.50 * 0.15 ~ 0.075 = 7.5% of GHI. The net result is that computed DNI may have a relative error of:

$$(\mathrm{GHI} \pm 1.5\%) - (\mathrm{DHI} \pm 7.5\% \ \{of\ GHI\}) \sim \pm 9\%.$$

Therefore, errors upwards of 7% to 9% can occur in the computation of DNI from GHI and DHI using silicon radiometers. The lower bound results if DHI is a smaller fraction (e.g, 10%) of the total GHI. Of course, random cancellation of errors over longer intervals will help reduce the overall uncertainty in averaged data. But for high time resolution data, there can be a significant spectral impact on GHI and DHI measurements, depending on atmospheric conditions during calibrations and measurements.

GHI corrections for silicon radiometers derived by King (2), based on air mass, were empirically derived for a relatively high-altitude, clear Western site (Albuquerque, New Mexico) and are probably site- (and spectral-content) specific. Unless site-specific comparison measurements between broadband thermal detectors and narrow-band silicon detectors are used to develop site-specific corrections to silicon GHI and DHI data, larger uncertainties must be assigned to silicon radiometer GHI, DHI, and derived DNI data. Although relatively good performance of rotating shadowband radiometers and GHI silicon photodectors is documented (9, 10), it is imperative to remember the units evaluted are generally calibrated and used for routine measurements at the same location.

5. SUMMARY

SMARTS 2.9.5 modeled relative spectral distribution of DHI sky radiation and total global hemispherical irradiance as seen by a typical silicon PD radiometer were analyzed. Spectra for a sea-level and a high-altitude site over a range of air masses and two atmospheric conditions (low aerosol optical depth and water vapor and high aerosol optical depth and water vapor) were modeled. Differences in the ratio of the effective solar irradiance to total solar irradiance ratios for each site are on the order of 2% in effective-to-total GHI ratios and 6% or more in effective-to-total DHI irradiances. Empirical corrections derived at each of the sites, to arrive at a total DHI, can differ by up to 60%. The net result is that error of upwards of 7% to 9% may occur in the computation of DNI from GHI and DHI using silicon radiometers in rotating shadowband radiometers. Empirical corrections (e.g., by comparison to thermal sensors measuring DHI) derived at one site may not be applicable at another, substantially different site.

6. NOMENCLATURE

Air mass (AM): The relative path length through the atmosphere, with respect to the vertical, of the direct beam radiation. AM equals the reciprocal of the sine (cosine) of the solar elevation (zenith) angle.

Aerosol optical depth: Dimensionless parameter representing transparency of the atmosphere as affected by small particles. The negative logarithm of relative amount of

direct beam radiation transmitted (not absorbed or scattered) in the beam path through the atmosphere. Usually with respect to the vertical path, or AM =1.

Diffuse hemispherical irradiance (DHI): Diffuse or total hemispherical sky radiation incident on a horizontal surface with the solar disk blocked in watts/square meter (Wm^{-2}).

Direct normal irradiance (DNI): Direct normal or direct "beam" irradiance. Radiation within a 5° field of view centered on the sun intercepted by a surface perpendicular to the surface (the "normal" vector) pointed at the center of the sun (Wm^{-2}).

Effective irradiance: For a detector with spectral response smaller than the total span of solar spectral irradiance, that portion of the total spectrum to which the detector responds, in units of integrated spectral power in Wm^{-2}.

Global hemispherical irradiance (GHI): Total hemispherical radiation on a horizontal surface, sometimes referred to as "global" horizontal radiation (Wm^{-2}).

Precipitable water: The total equivalent depth, in centimeters, of water vapor condensed from a vertical column in the atmosphere. Units of atmosphere-cm (atm-cm).

Pyranometer: Radiometer for measuring GHI (unshaded) or DHI (shaded from direct beam radiation).

Pyrheliometer: Radiometer for measuring DN, sometimes referred to as "normal incident pyrheliometer."

Responsivity (Rs): The signal generated by a radiometer (generally microvolts, μV, or millivolts) per unit of incident radiation, e.g., $\mu V/(Wm^{-2})$. The reciprocal of responsivity is the calibration factor, Cf, $Wm^{-2}/\mu V$.

Reference irradiance: High-quality solar irradiance, based on low-uncertainty instruments, or computed from low-uncertainty instruments, such as GHI from DNI and DHI.

Rotating shadowband radiometer: Instrument with an unshaded pyranometer to measure GHI and shaded with a rotating band to measure total sky DHI radiation, from which DNI is computed.

Silicon photodiode detector: Silicon-based solid state detector, typically operating in photovoltaic mode, generating a current proportional to the irradiance.

Spectral correction: An adjustment factor, usually empirically derived, to shift measured broadband data to account for spectral effects different from calibration conditions.

Spectral response: The variation in the output signal of a radiometer as a function of the wavelength of light being measured.

Thermal detector: Detector that absorbs optical radiation and produces a thermal signal (rise in temperature) that can be detected and recorded.

Zenith angle, Z: Angle between the foot of the local vertical ("zenith direction") and the center of the solar disk. Complement of the solar elevation angle.

Zenith angle or angle of incidence correction: Correction to account for variations in responsivity, Rs, as a function of zenith and or incidence angle.

7. ACKNOWLEDGMENTS

This work was performed under DOE prime contract number DE-AC36-08-GO28308.

8. REFERENCES

(1) Michalsky, J.J, Harrison, L., Lebaron, B.A., "Empirical Radiometric Correction of a Silicon Photodiode Rotating Shadowband Pyranometer," *Solar Energy* 39(2): 87-96, 1987

(2) King, D.L., Myers, D.R., "Silicon-Photodiode Pyranometers: Operational Characteristics, Historical Experiences, and New Calibration Procedures," Proceedings 26th IEEE Photovoltaic Specialists Conference, Sept. 29–Oct 3, 1997, Anaheim, California, 1997

(3) Vignola, F., "Removing Systematic Errors From Rotating Shadowband Pyranometer Data," Proceedings of American Solar Energy Society Annual Conference July 9–13, 2006, Denver, Colorado, 2006

(4) WMO, *Guide to Meteorological Instruments and Methods of Observation*, WMO No. 8. 7th Ed., World Meteorological Organization, Geneva, Switzerland, 2008

(5) Gueymard, C.A., Myers, D.R., "Evaluation of Conventional and High Performance Routine Solar Radiation Measurements for Improved Solar Resources, Climatological Trends, and Radiative Modeling," *Solar Energy* 83, pp. 171–185, 2009

(6) Stoffel, T., et al., *Concentrating Solar Power Best Practices Handbook for the Collection and Use of Solar Resource Data*, National Renewable Energy Laboratory technical report, NREL/TP-550-47465, September 2010

(7) Gueymard, C., “Parameterized Transmittance Model for Direct Beam and Circumsolar Spectral Irradiance,” *Solar Energy* 71(5): 325–346, 2001

(8) Anon., *Li-COR Radiation Sensors Instruction Manual*, Terrestrial Type SA, Li-COR Inc., Lincoln, Nebraska, 1991

(9) Geuder, N., Pulvermuller, B., Vorbrugg, O., “Corrections for Rotating Shadowband Pyranometers for Solar Resource Assessment,” Proceedings of SPIE Conference 7046, Optical Modeling and Measurements for Solar Energy Systems II, August 13–14, 2008, Society for Photo-Optical Instrumentation Engineers, Bellingham, Washington, 2008

(10) Wilcox, S.M., Myers, D., “Evaluation of Radiometers in Full-Time Use at the National Renewable Energy Laboratory Solar Radiation Research Laboratory,” National Renewable Energy Laboratory technical report, NREL/TP-550-44627, December 2008